OVERVIEW OF RESEARCH RESULTS FROM THE ALCATOR C-MOD TOKAMAK

E. S. MARMAR and the Alcator C-Mod Team
MIT Plasma Science and Fusion Center
Cambridge MA 02139 USA
Email: marmar@mit.edu

Abstract

Alcator C-Mod is the only divertor tokamak in the world capable of operating at magnetic fields up to 8 T, equaling and exceeding that planned for ITER, and comparable to those envisioned for compact, high field tokamak reactors. Because of its relatively compact size, C-Mod accesses regimes of extreme edge power density (1 MW/m^2 average through the surface of the plasma. The highest pedestals are obtained by accessing the super H-mode regime predicted by EPED, enabling C-Mod to demonstrate P_{ped} at 90% of the ITER target. Data from a multi-machine database shows that the boundary heat flux width scales inversely with B_θ, independent of machine size. The most recent data have extended this scaling to B_θ=1.3 T, beyond that envisioned for ITER, and the B_θ^{-1} scaling persists. Based on these results, it is clear that power handling in reactors will be an even bigger challenge than in ITER, arguing for the urgent need for one or more dedicated Divertor Test Tokamaks (DTT), such as the ADX. UEDGE simulations of long-leg divertor configurations, which could be tested in a DTT, show a possible stable detached divertor solution in a high-field reactor design with exhaust power approaching 100 MW. Laser blow-off induced cold-pulses, an enigmatic transient phenomenon that has challenged the standard local-transport paradigm, has been explained by a new local turbulent transport model. Results from the TRANSP power balance code, coupled to the quasilinear transport model TGLF-SAT1, with a new saturation rule that came about as a consequence of cross-scale coupling physics, and that captures the nonlinear upshift of the critical gradient, are shown to describe the cold-pulse, including the existence of core temperature inversions at low density and disappearance at high density. A Random Forests Machine Learning algorithm has been trained on thousands of C-Mod discharges to detect disruption events. Disruption evolution time scales on C-Mod are relatively short; based on a time-slice approach, reliable warnings are found only a few ms before disruption. However, a shot-by-shot approach gives improved prediction reliability. Steady-state tokamak reactors will need high bootstrap fraction, supplemented by RF current drive. Lower Hybrid Current Drive is among the most efficient non-inductive techniques. Recent modeling indicates that moving the launch point to the high field side can have many benefits, including accessibility at lower $n_\parallel$ for higher current drive efficiency. C-Mod experiments have explored access to H-mode and I-mode at magnetic fields approaching 8T. Results at up to 8 T confirm that the L–I power threshold varies only weakly with field, and that the power range for I-mode increases with field. H-modes on C-Mod have achieved world-record tokamak volume-average and pedestal plasma pressures (<P> above 0.2 MPa, Pped ~ 80 kPa).

1. INTRODUCTION

Alcator C-Mod [1.1, 1.2, 1.3] is a compact, high-field tokamak, whose unique design and operating parameters have produced a wealth of new and important results, contributing data that extend tests of critical physical models into new parameter ranges, and into new regimes. During more than 23 years of operation, Alcator C-Mod produced over 35,000 plasma discharges with a startup reliability of 80%. The engineering reliability, as defined by all systems operating properly during the plasma attempt, was over 96%. Using only high-power radio frequency (RF) waves for heating and current drive, with innovative launching structures, C-Mod operated routinely at reactor level power densities and achieved plasma pressures higher than any other toroidal confinement device. During its last plasma operation day, Alcator C-Mod broke its own world's record volume average plasma pressure, achieving 0.2 MPa, a record which is unlikely to be exceeded by any currently operating tokamak.

C-Mod spearheaded the development of the vertical-target divertor, and has always operated with high-Z metal plasma facing components --- approaches subsequently adopted for ITER and likely to be applied in any power-producing reactor. C-Mod has made ground-breaking discoveries in divertor physics and plasma-material interactions at reactor-like power and particle fluxes, and elucidated the critical role of cross-field transport in divertor operation, edge flows and the tokamak density limit. C-Mod developed the I-mode and the Enhanced Dα H-mode regimes, which have high performance without large edge localized modes, and with pedestal transport self-regulated by short-wavelength electromagnetic waves. C-Mod has carried out pioneering studies of intrinsic rotation and demonstrated that self-generated flow shear can be strong enough in some cases to significantly modify transport. C-Mod made the first quantitative link between the pedestal temperature and I-mode performance, showing that the

observed self-similar temperature profiles were consistent with critical-gradient-length theories, and followed up with quantitative tests of nonlinear gyrokinetic models. RF research highlights include direct experimental observation of ion cyclotron range of frequency (ICRF) mode-conversion. ICRF flow drive, demonstration of lower-hybrid current drive at ITER-like densities and fields, and, using a set of novel diagnostics, extensive validation of advanced RF codes. Disruption studies on C-Mod provided the first observation of no-axisymmetric halo currents, and non-axisymmetric radiation in mitigated disruptions. Because of its relatively compact size, C-Mod accesses regimes of extreme edge power density (1 MW/m^2 average through the surface of the plasma). Scrape-off layer (SOL) power widths are as small as 0.5 mm, with measured parallel power flows >1 GW/m^2 at the divertor, surpassing the design for ITER, and approaching the levels envisioned in pilot and DEMO power plants. C-Mod results are particularly important for providing the physics basis of the high-field, compact tokamak approach, which can lead to a faster path in the development of fusion energy. A particular emphasis of the 2016 run campaign was to make full use of the facility capabilities, including extensive operation at maximum magnetic field.

This overview presents analysis of experiments from the final C-Mod campaigns, spanning multiple science topics, including: core energy, particle and momentum transport (Section2); pedestal dynamics (Section 3); RF heating and sustainment (Section 4); boundary and SOL physics (Section 5); and disruptions (Section 6).

2. CORE TRANSPORT

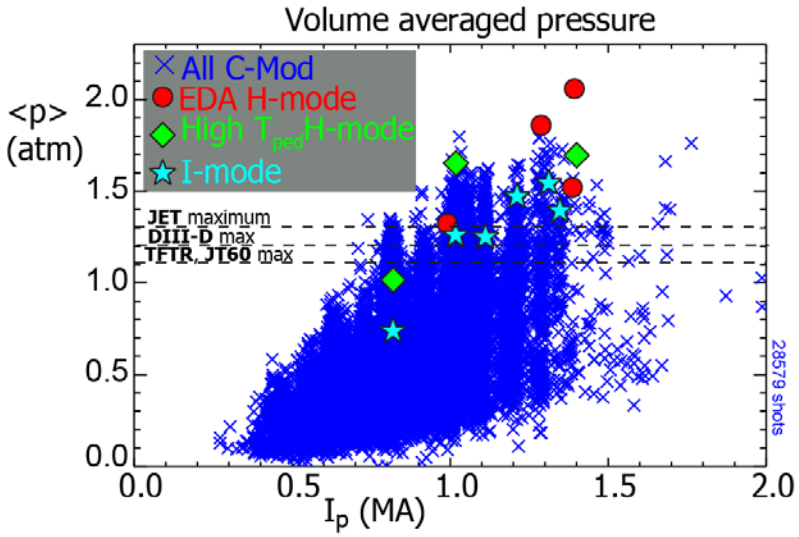

Fig. 1.1 Volume average pressure as a function of plasma current, across all C-Mod operational regimes.

Fusion reactivity does not depend explicitly on β, but rather is approximately ∝ (plasma pressure)^2, and high field offers the intrinsic advantage of high pressure at moderate β, which in turn generally leads to enhanced stability. Figure 1.1 shows the achieved volume average pressure from selected discharges in the entire C-Mod database, which includes L-mode, I-mode, and H-mode operation, including ohmic and ICRF auxiliary heating. High performance is achieved in ELMy and EDA H-mode, in I-mode, and high T_e pedestal ("super") H-mode.

Recent core transport physics studies have focused on multi-scale turbulence interactions, the influence of trapped electron modes on core energy transport, the LOC/SOC transition, understanding I-mode, intrinsic rotation, impurity transport, fluctuation diagnostics, stiffness/critical gradients and uncertainty quantification.
Multi-scale turbulence: multi-scale gyrokinetic simulations that capture ion and electron scale turbulence simultaneously have revealed the dynamics of cross scale energy transfer and zonal flow modification that give rise to heat losses. These computationally expensive simulations have provided a likely explanation for the great unsolved problem of electron heat loss in tokamak plasmas.

Trapped Electron Modes: Density gradient driven trapped electron modes were found to dominate inner core transport in moderately peaked H-mode plasmas in both C Mod and DIII-D, allowing local control of density peaking with electron heating. Gyrokinetic simulations reproduce the particle, electron thermal, and ion thermal energy fluxes in the experiments within measurement uncertainty. Nonlinear gyrokinetic simulations using GS2, carried out for Alcator C-Mod experiments, revealed that the effective critical density gradient above which TEM turbulent transport becomes stiff lies well above the linear threshold for instability at high collisionality. This non-linear upshift in the Trapped Electron Mode (TEM) critical density gradient is associated with zonal flow dominated states, and increases strongly with collisionality. Alcator C-Mod experiments are consistent with this prediction – the H-mode ITB density gradient is effectively limited by the TEM nonlinear critical density gradient during on-axis heating, which arrests density peaking as it increases with time.

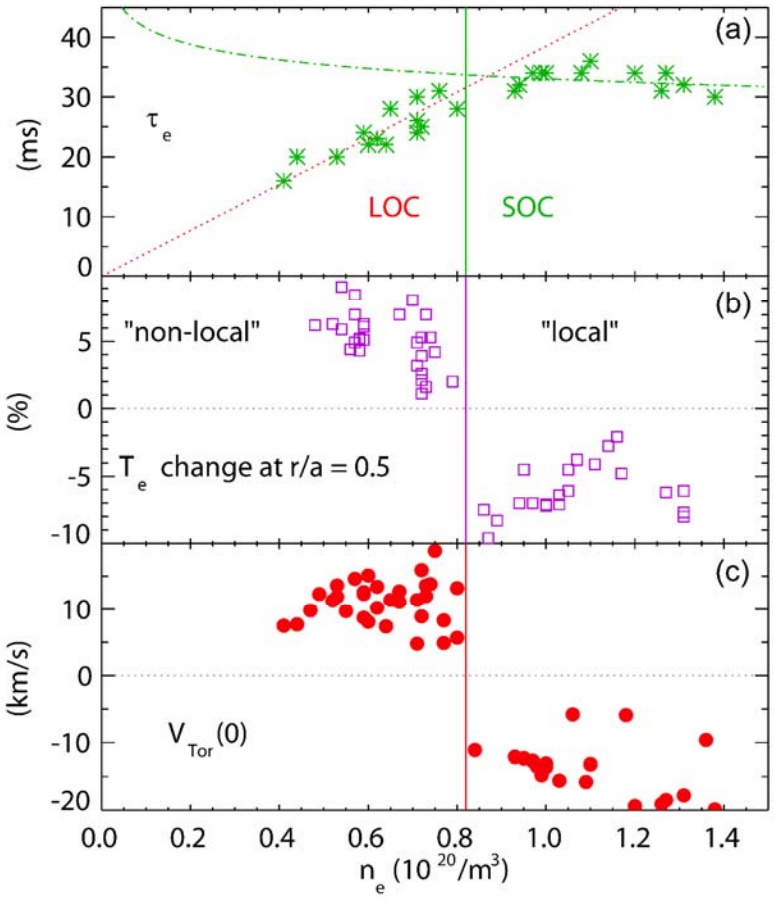

Fig. 2.2 Density dependence of plasma responses across the LOC/SOC boundary: a) scaling of t_e; b) T_e response at r/a=0.5 after edge impurity injection, showing the "non-local" ~5% temperature rise in the LOC regime; c) reversal of intrinsic core rotation across the boundary.

The LOC/SOC transition: Several phenomenological transformations occur at the LOC/SOC transition-rotation reversals, 'non-local' cutoff and turbulence changes. The disappearance of measured electron temperature fluctuations in going from LOC to SOC has been captured in gyrokinetic simulations. The 'non-local' cutoff in cold pulse propagation can be explained without invoking non-local effects. Figure 2.2 shows the variations in key parameters as a function of plasma density across the LOC to SOC transition for a series of 800 kA, 5.3 tesla discharges.

Laser blow-off induced cold-pulses, an enigmatic transient phenomenon that has challenged the standard local-transport paradigm, has been explained by a new local turbulent transport model [2.1]. Results from the TRANSP power balance code, coupled to the quasilinear transport model TGLF-SAT1 [2.2], with a new saturation rule that came about as a consequence of cross-scale coupling physics, and that captures the nonlinear upshift of the critical gradient, are shown to describe the cold-pulse, including the existence of core temperature inversions at low collisionality and disappearance at high collisionality. By means of experimentally-constrained self-consistent modeling of C-Mod cold-pulse experiments, this work provides the strongest evidence to date that the existence of non-local transport phenomena may not be necessary for explaining the behavior and timescales of cold-pulse experiments in tokamak plasmas.

Understanding I-mode: Long wavelength density and temperature fluctuations in the core are found to decrease significantly at the L- to I-mode transition. Non-linear gyrokinetic simulations suggest that ExB shearing and increased profile stiffness are responsible for the reduction in turbulence.

Intrinsic rotation: The magnitude and scaling of intrinsic toroidal rotation in H- and I-mode plasmas agrees with the predictions of a fluctuation entropy balance model which gives a Mach number proportional to ρ*. In plasmas with LHCD, the direction of the rotation depends upon the value of q_0, with co-current rotation see in discharges

with significant current drive. In L-mode plasmas, rotation reversals cannot be due to changes in electron kinetic profile second derivatives.
Impurity transport: Impurity confinement has been characterized in L-, I- and H-mode plasmas, with the confinement time proportional to the pedestal density gradient across all regimes. The insensitivity of impurity transport to rotation profile shape in ICRF heated L-mode plasmas is captured in gyrokinetic simulations.
Temperature and density fluctuation diagnostic development: A CECE diagnostics has been built for C-Mod enabling measurement of spatially localized electron temperature fluctuations, for direct comparison to gyrokinetic simulations. In addition, a fast TCI diagnostic has been fabricated for looking at long wavelength density fluctuations.
Stiffness/critical gradients: Electron temperature profile stiffness has been explored by two different methods- analyzing heat pulse propagation by use of partial sawteeth and by using magnetic field jogs to sweep the radial coverage of ECE. Comparison with gyrokinetic simulations suggests that ETG mode turbulence is important in determining the electron temperature profile shape.
Uncertainty quantification: Gaussian process regression has been used to obtain rigorous error bars in kinetic profiles, including gradients and 2nd derivatives, with a variety of applications.

3. PEDESTAL DYNAMICS

H-modes on C-Mod have achieved world-record tokamak volume-average and pedestal plasma pressures (<P> above 0.2 MPa, P_{ped} ~ 80 kPa)[3.1]. Fig. 3.1 shows measured P_{ped} compared to model predictions. The highest pedestals are obtained by accessing the super H-mode regime predicted by EPED [3.2] enabling C-Mod to demonstrate P_{ped} at 90% of the ITER target. C-Mod also achieved ~60kPa pressure pedestals in stationary ELM-suppressed plasmas (black squares in the figure), and this is also higher than any other device's maximum pressure pedestal.

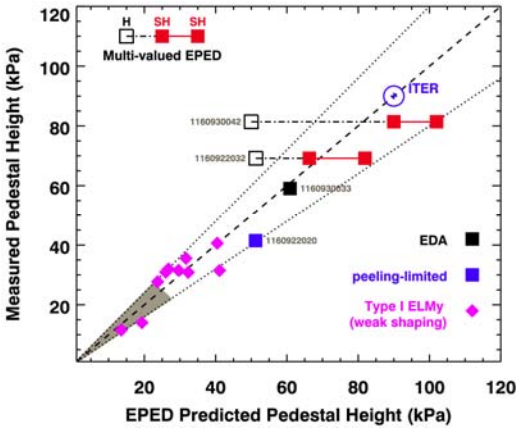

Fig. 3.1 Comparisons of P_{ped} with EPED predictions.

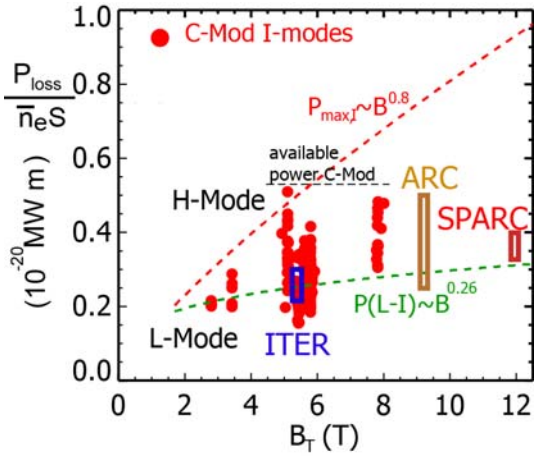

Fig. 3.2 I-mode operation in C-Mod in the space of power/area vs. toroidal field. Also shown are predictions for ITER, and two future concepts, SPARC and ARC.

The intrinsically ELMless I-mode regime [3.3] shows significant promise for next step/burning plasma devices. Operation at high B_T on C-Mod show that the power window for I-mode access widens, as seen in figure 3.2. Also shown in the figure are extrapolations for expected operational ranges of two concepts, SPARC [3.4] which aims at net energy production, and ARC [3.5], a prototype power reactor concept, along with expectations for ITER.

Experimental studies of the L-H transition on Alcator C-Mod have strengthened the basis for projecting power requirements for future fusion devices. On C-Mod, L-H experiments at toroidal field BT of 4.0—7.8T reveal that H-mode power threshold Pth accords roughly with projections from a scaling law used to determine power needs for ITER [3.6, 3.7]. However, as on numerous devices, the scaling law does not capture the experimental density dependence of Pth at low normalized density, and at moderate to high density the inferred experimental Pth does not scale as strongly with BT as the scaling law would indicate. We can partially resolve these discrepancies by performing transport and power balance analysis of C-Mod plasmas just prior to L-H transitions [3.8]. Analysis confirms and extends a key result found on ASDEX Upgrade (AUG): a critical value of surface-integrated ion heat flux per particle Qi/n is necessary to enable the transition from L-mode to H-mode [3.9]. The C-Mod study considers discharges at ITER-relevant field and density, and indicates that Qi at the L-H transition not only increases linearly with n but also increases with BT. The n, BT scalings are not directly reflected in Pth because of changing balance

of edge electron and ion heat fluxes, which depends in turn on the auxiliary heating scheme and the strength of electron-ion equilibration. Combining data from C-Mod and AUG yields a general expression for the edge ion heat flux Qi/S at the L-H transition: qi=0.0021n1.07B0.76. The expression is sensible when compared to the ITER Pth scaling law [3.10], and provides an additional means of projecting H-mode power requirements to ITER. Because C-Mod areal power densities actually exceed that of ITER, the projection to ITER is an interpolation in the C-Mod/AUG database, rather than an extrapolation.

4. HEATING AND CURRENT DRIVE

Efficient current sustainment in tokamak reactor regimes remains a significant technical challenge on the path to commercial fusion energy. It is likely that reactors will need high bootstrap fraction, supplemented by RF drive. Although among the most efficient non-inductive techniques, Lower Hybrid Current Drive (LHCD) can be challenged by rapid fall-off in efficacy and wave penetration at reactor-relevant plasma parameters. Experiments on C-Mod indicate that the root cause for the decrease in efficacy at reactor relevant densities is wave interaction with the SOL, which can be avoided by managing the SOL[4.1]. Recent modeling indicates that moving the launch point to the high field side can have many benefits, including accessibility at lower $n_{\parallel}$ (giving higher η_{CD}) while reducing edge plasma and wall interactions[4.2].

Among the most important issues for LHCD is the reduction in LHCD efficiency at high density that has been a ubiquitous feature of LHCD experiments worldwide.[4.3, 4.4, 4.5] For C-Mod, the LHCD efficiency had degraded when line average n_e exceeds ~1.0×10^{20} m^{-3}. At low to moderate density (line averaged $n_e < 1\times10^{20}$ m^{-3}), LHCD is highly efficient with an efficiency, $\eta \equiv n_e I_{LH} R_0 / P_{LH}$, of 2-$3\times10^{19}$ A/Wm^2. Early observations in current drive efficiency degradation at high density [4.6] identified the plasma edge and SOL as the region where the LH waves deposit their energy, rather than in the plasma core as anticipated. Subsequent work has focused on the mechanisms by which the LH waves are absorbed at high density. Collisional absorption in the SOL [4.4] and parametric decay instabilities (PDI) [4.7] are two possible mechanisms; they are both enabled by weak, multi-pass absorption of the LH waves in the discharges of interest.

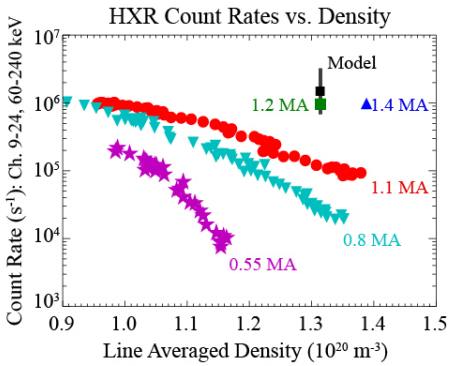

Fig.4.1 With increasing plasma current, the hard X-ray counts increase for high density. At 1.2 MA, the total HXR count is consistent with the model. The range of model values results from the uncertainties in the electric field distribution in the plasma.

Detailed experiments, for the first time, quantified the power deposition of lower hybrid RF waves into the edge plasma of a diverted tokamak. Using a unique set of fast time resolution edge diagnostics, including innovative fast-thermocouples, an extensive set of Langmuir probes, and a Lyman alpha ionization camera, the toroidal, poloidal, and radial structure of the power deposition were simultaneously determined. Power modulation was used to directly isolate the RF effects due to the prompt ($t<\tau_E$) response of the scrape-off-layer (SOL) plasma to LHCD power. LHCD power was found to absorb more strongly in the edge at higher densities and a majority of this edge-deposited power is promptly conducted to the divertor. This correlates with the loss of current drive efficiency at high density previously observed on Alcator C-Mod. Measurements of ionization in the active divertor show dramatic changes due to LHCD power, implying that divertor region can be a key for the LHCD edge power deposition physics.[4.8]

A path to improve LHCD efficiency at high density is to reduce the SOL density and associated fluctuations through raising the plasma current motivated by the previously identified scaling of the SOL characteristic to the Greenwald fraction. These experiments, as seen in figure 4.1, demonstrated efficient LHCD up to the line-averaged density ≈ 1.5×10^{20} m^{-3} in a diverted configuration exceeding the previously reported density limit at n_e ~1×10^{20} m^{-3}. By raising plasma current up to 1.4 MA at n_e≈ 1.4×10^{20} m^{-3}, parasitic interactions were largely eliminated, evidenced by a minimal broadening in the wave frequency spectrum. The injected LH power (600 kW) produced a loop voltage drop (ΔV = 0.2 V) consistent with engineering efficiency found at low density. Compared to the low current plasma that exhibited the "density limit", the non-thermal Bremsstrahlung emission rates increased significantly, and is consistent with simulation results. The new experimental results show that efficient current drive at a reactor density can be attained with proper management of the SOL

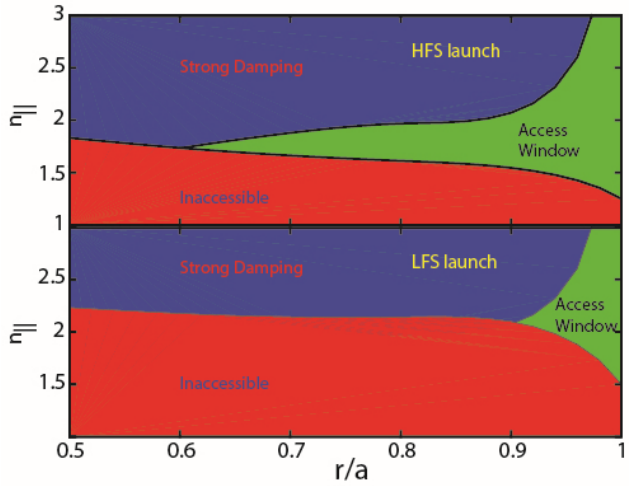

Fig. 4.2 Access window for HFS is dramatically improved compared to LFS LHCD launch using FDF profiles, B_0=6 T and 5 GHz waves.

The high field side (HFS) launch of LHCD power, particularly in double null configurations, has been found to represent an integrated solution that has the potential to both solve core wave physics challenges and mitigate PMI / coupling problems [4.2]. HFS LHCD launch opens the "accessibility window", allowing for use of a lower parallel refractive index, n//, for a given plasma density and on-axis magnetic field (see figure 4.2). The lower n// waves damp in a region of higher temperature, resulting in increased current drive efficiency and a damping profile shifted closer to the mid-radius as compared to low field side launch. Moving the LHRF antenna to the narrow, quiescent scrape off layer (SOL) on the HFS reduces the likelihood of detrimental parametric decay, wave scattering from density fluctuations, as well as ameliorating the plasma-material interaction and wave coupling challenges. Additional benefits with respect to fast particle and neutron fluxes can be realized by moving to the HFS.plasma. The improved LHCD core physics motivates an experimental effort to validate the HFS LHCD core and coupling physics in DIII-D planned for installation in 2020.

5. BOUNDARY AND SCRAPE-OFF-LAYER PHYSICS

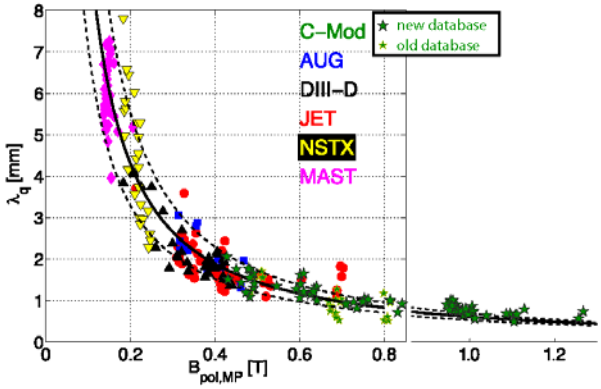

Fig. 5.1 Recent C-Mod data extends heat scrape-off width results to the ITER B_θ (1.2 T) and beyond.

Fig.5.2 ADX Divertor Test Tokamak conceptual design.

A major focus of the final experimental campaigns on Alcator C-Mod was to characterize the heat flux width, λ_q, over a wide range of conditions, utilizing a unique array of heat flux sensors with unprecedented spatial resolution and heat flux dynamic range. A major finding [5.1] is that the inverse poloidal heat flux width scaling was found to extend up to B_θ~1.3 T in H-mode (see figure 5.1), and also in I- and L-mode. Across all confinement modes, $l_q \propto 1/\langle pressure \rangle$. Based on these results, it is clear that power handling in reactors will be an even bigger challenge than in ITER, arguing for the urgent need for one or more dedicated Divertor Test Tokamaks (DTT), such as the ADX design[5.2] (fig.5.2). Recent modeling indicates that long-legged divertors can achieve stable detachment away from the core plasma for a large power window, especially those employing an embedded X-point [5.3, 5.4]. These geometries, which can be tested in a DTT (see fig. 5.3), are compatible with the space constraints and shielding

requirements of a high-field, compact tokamak pilot plant [5.5] and appear to accommodate the power exhaust with minimal impurity seeding, even accounting for the narrow heat flux widths [5.6].

Another area of focus was an examination of the power sharing among divertors as the magnetic topology was varied from single-null to balanced double null [5.7]. It was found that power sharing amongst the outer (upper versus lower) and inner (upper versus lower) pairs of divertors can be described in terms of a logistic function of magnetic flux balance, consistent with heat flux mapping along magnetic field lines to the outer midplane. The overall behavior of H-modes operated near double null and for I-modes operating to within one heat flux e-folding of double null were found to be similar to Ohmic L-modes, with a significant reduction of power on the inner divertor legs. In addition, heat flux footprints and power e-folding widths, λ_q, on the inner divertor in I-modes were explored. It is found that these λ_q are slightly larger than those obtained on the outer divertor but similarly tend to follow an inverse scaling with poloidal magnetic field strength.

The effect of divertor nitrogen seeding on scrape-off layer heat flux widths was explored during the FY15 and FY16 run campaigns making use of a new feedback control technique to inject nitrogen in the C-Mod divertor [5.8]. It is found that the SOL power e-folding width is robustly insensitive to divertor conditions, spanning the range of sheath-limited to high-recycling to near detached conditions with parallel heat flux at the divertor target varying by a factor of ~10. These results challenge the idea that divertor conditions affect plasma turbulence and transport 'upstream' (and thus λ_q) and have important implications for the use of advanced divertor configurations, such a long-leg divertors.

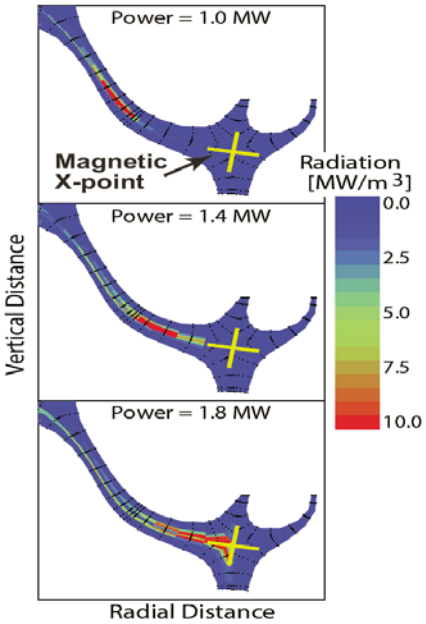

Fig. 5.3 Modeling of a double-null, long-leg X-point divertor for ADX-like parameters. Detachment is stable over a large range of parallel power into each divertor.

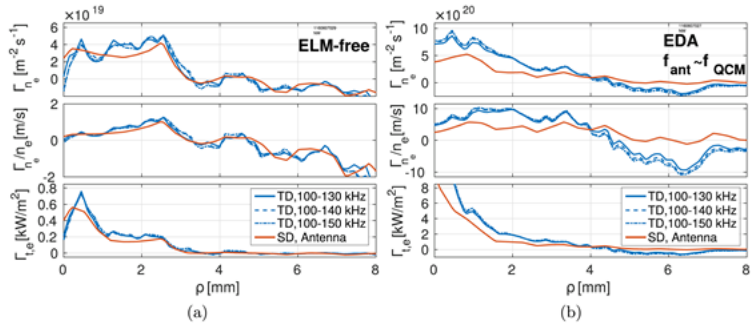

Fig. 5.4 Profiles of radial transport of particles (Γ_n, Γ_n/n_e) and energy ($\Gamma_{t,e}$) driven by a QCM-like mode driven by the Shoelace antenna during ELM-free (left) and EDA phases (right) of ohmic H-mode plasmas. Mirror Langmuir probe data are analyzed using time domain analysis (TD) in three frequency bands and via a spectral domain (SD) analysis. ρ is the distance from the last closed flux surface at the outer mid plane.

The Shoelace antenna was built to drive edge fluctuations in the Alcator C-Mod tokamak, matching the wavenumber ($k \sim 1.5\ cm^{-1}$) and frequency ($30 < f < 200$ kHz) of the quasi-coherent mode (QCM), which is responsible for regulating transport across the plasma boundary in the steadystate, ELM-free Enhanced Dα (EDA) H-mode. In 2016, the Shoelace antenna was relocated to enable direct measurements of driven transport by a reciprocating Mirror Langmuir Probe, while also making available gas puff imaging and reflectometer data to provide additional radial localization of the driven fluctuation.[5.9] These new data suggest a 4 mm-wide mode layer centered on or just outside the separatrix. Fluctuations coherent with the antenna produced a radial electron flux with $\Gamma_e/n_e \sim 4$ m/s in EDA H-mode, smaller than, but comparable to the QCM level. But in transient ELM-free H-mode, Γ_e/n_e was an order of magnitude smaller, and driven fluctuations reduced by a factor of 3.(See figure 5.4) The driven mode is quantitatively similar to the intrinsic QCM across measured spectral quantities, except that it is more coherent and weaker. This work informs the prospect of achieving control of edge transport by direct coupling to edge modes, as well as the use of such active coupling for diagnostic purposes.

6. DISRUPTIONS: RUNAWAY GENERATION AND DISRUPTION PREDICTION

In addition to interrupting power production, major disruptions have several potentially deleterious effects, including runaway electrons and large vessel forces due to image and halo currents. The study of the threshold electric field to generate relativistic runaway electrons (RE's) on C-Mod revealed that synchrotron emission was a major energy loss mechanism. This is a consequence of Alcator C-Mod's high magnetic field, which also results in the RE synchrotron radiation being emitted strongly in the visible wavelength range. Absolutely-calibrated spectrometers, distortion-corrected cameras, and the Motional Stark Effect (MSE) diagnostic have been used to measure synchrotron spectra, images, and polarization information, respectively. The new synthetic diagnostic SOFT [6.1] has been used to simulate all three measurements, with the first work on C-Mod images published in [6.1] and the most complete work on spectra published in [6.2]. Spectra were measured at three magnetic fields (2.7, 5.4, and 7.8 T), and a test particle model of RE energy and density was input into SOFT to reproduce experimental data. The data were consistent with RE energies decreasing as magnetic field was increased, motivating further exploration of high-field tokamaks.

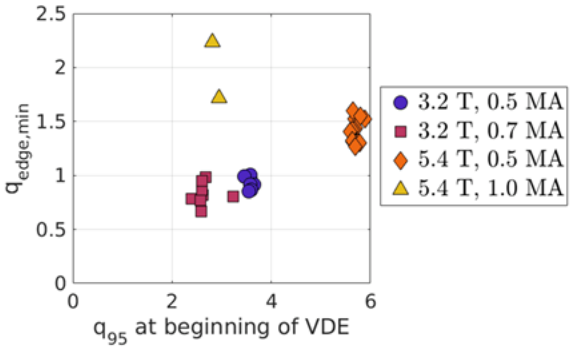

Fig. 6.1 Many VDEs are found to terminate at approximately rational minimum q_{95} values of ~1 and ~3/2.

In Alcator C-Mod triggered vertical displacement events, plasmas moved downward and contacted the first wall. Halo currents were measured with a set of outboard divertor Langmuir "rail" probes, which have high poloidal resolution (~1 cm spacing), while still having a large collection area. The plasma contact point on the divertor plate and its downward motion were clearly seen from positive and negative currents measured. Magnetic reconstructions of the plasma boundary matched probe data and were used to calculate the edge safety factor, which was found to decrease to approximately rational values (~1 and 3/2) before disruption (see figure 6.1). Finally, from reproduced VDEs, the halo region temperature was estimated to be ~35-60 eV, which is consistent with previous simulations and can guide future ones [6.3].

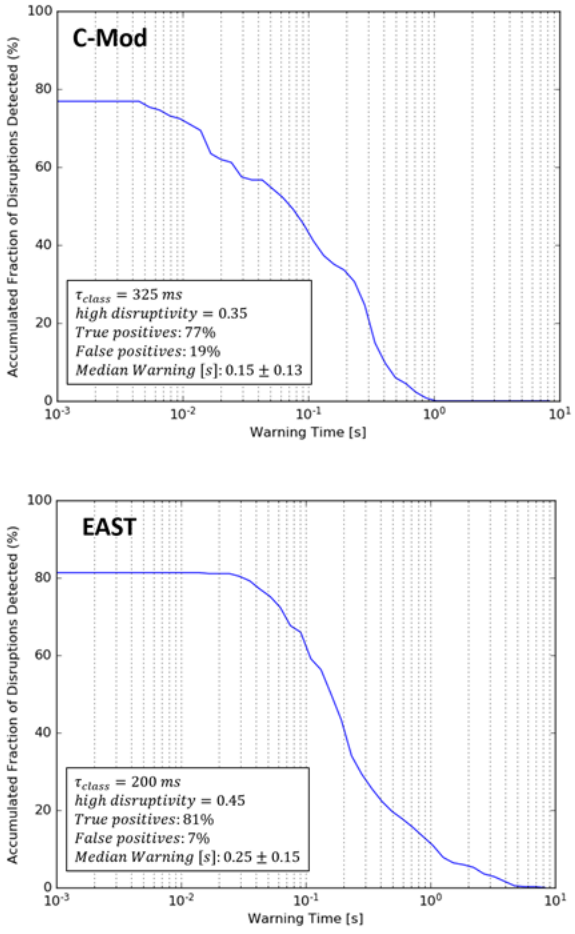

Fig 6.2 Cumulative fraction of test set disruptions detected with at least the given warning time for Alcator C-Mod and EAST; the legend boxes state the class label time and high disruptivity threshold for the best operational point, as well as the true and false positive rates.

In recent years, there has been a concerted effort to establish disruption databases for C-Mod and other tokamaks, and to apply artificial intelligence to develop disruption prediction capability by training machine learning algorithms on these databases. We have been extensively developing disruption prediction algorithms based on the Random Forest AI method, and trained on our C-Mod, DIII-D, and EAST databases[6.4]. We are finding that the plasma parameters that are most relevant for

disruption prediction are different on the different machines. Furthermore, the prediction success rates for Random Forests trained on each machine database varies significantly on a timeslice-by-timeslice basis. However, on a shot-by-shot basis, the optimized Random Forests algorithms have quite similar success rates for predicting impending disruptions (77% for C-Mod and 81% for EAST), as shown in figure 6.2.

7. APPENDIX: SIGNATURE ACHIEVMENTS OF THE ALCATOR C-MOD PROGRAM

Over its operational history, many signature achievements have come from the Alcator C-Mod facility. The top results include:

1) C-Mod is the highest field, diverted tokamak in the world with operation at 8 T and 2 MA.[7.1]
2) Demonstrated tokamak initiation and control with a solid conducting vessel and structure.[7.2]
3) Set world-record P/S power densities of ~1 MW/m^2, producing reactor-level SOL parallel heat flux densities approaching 1 GW/m^2.[7.3]
4) Demonstrated the feasibility of a very high-power tokamak operation with a high-Z divertor and plasma facing components, including measurement of erosion and fuel retention rates. [7.4, 7.5, 7.6, 7.7]
5) Invented and established the vertical plate divertor as most favorable for power and particle handling and explored divertor regimes at reactor-like plasma parameters including the neutral-neutral collisionality, neutral opacity, and photon opacity. [7.8, 7.9, 7.10]
6) Discovered "main-chamber recycling" phenomenon in C-Mod's diverted plasmas and revealing intermittent, non- diffusive transport in the scrape-off layer as the underlying cause.[7.11]
7) Demonstrated controlled divertor detachment using seeded impurities at high power density and demonstrated good H-mode confinement, H98~1, with Demo-like fractions (90%) of radiated power. [7.12, 7.13, 7.14]
8) Uncovered evidence for the marginal stability paradigm for SOL turbulent transport with a critical B_P gradient decreasing at higher collisionality. [7.15, 7.16]
9) Identified edge plasma transport and its scaling with collisionality as a key physics ingredient in the empirical tokamak density limit. [7.17, 7.18]
10) Demonstrated that spatial asymmetries in turbulence and transport drive near-sonic parallel plasma flows in the plasma edge, imposing a toroidal rotation boundary condition for the confined plasma—suggesting a mechanism for the ∇B drift asymmetry in the L-H threshold. [7.19, 7.20]
11) Carried out the first experiments that characterized the L-H threshold as a critical local temperature or temperature gradient. [7.21, 7.22]
12) Demonstrated the two stationary ELM-free regimes, the EDA H-mode and I-Mode, where particle and impurity confinement were controlled by continuous, short wave- length electromagnetic modes in the pedestal. [7.23, 7.24, 7.25]
13) Demonstrated the quantitative link between pedestal height and core performance across a wide range of operating conditions, validating the theoretically predicted dependence of turbulence on R/LT.[7.26, 7.27]
14) Discovered and explored large self-generated toroidal flows in the core plasma. [7.28, 7.29]
15) Demonstrated creation of Internal Transport Barriers via self-generated plasma flows and demonstrated transport control with on-axis RF heating, identifying TEM turbulence via first direct comparison of experiment to nonlinear gyrokinetic simulations processed with synthetic diagnostic. [7.30, 7.31, 7.32, 7.33, 7.34]
16) Validated gyrokinetic models simultaneously for ion energy, electron energy, and particle transport through groundbreaking, multi-scale simulations. [7.35, 7.36]
17) Proved experimentally that impurity asymmetry on flux surfaces occurs through mechanisms other than centrifugal force. [7.37, 7.38]
18) Carried out extensive studies of the spectroscopy and atomic physics of highly ionized atoms, including high n transitions and satellites, critical for development of plasma diagnostics and validation of atomic physics codes. [7.39]
19) Operated ICRF systems routinely at power densities above 10 MW/m^2. [7.19]S.J.Wukitch,M.L.Garrett,R.Ochoukov,J.L.Terry,A.Hubbard,B.Labombard,C.Lau,Y.Lin,B.Lipschultz,D.Milleretal.,

20) Validated full-wave ICRF models by comparison with measured wave fields, fast particle distributions, and local heating. [7.41, 7.42, 7.43, 7.44, 7.45]
21) Demonstrated RF flow drive by ICRF mode conversion. [7.46]
22) Pioneered the field aligned-antenna concept that dramatically reduced high-Z impurity levels in ICRF heated plasmas. [7.47]
23) Demonstrated efficient off-axis current drive with lower hybrid. [7.48, 7.49]
24) Developed the first full-wave LH codes, using these to explain the decrease in current drive efficiency at high densities. [7.50 – 7.54]
25) Showed the importance of spatial asymmetries and fast dynamics for disruption halo currents and disruption mitigation radiation. [7.55, 7.56]
26) Advanced the state-of-the-art for diagnosing the core, edge, and SOL plasma and plasma-material interactions.
27) Developed MDSplus, a data acquisition and data management system that has become the world standard for fusion experiments.
28) Established and then repeatedly broke the record for volume average pressure in a tokamak plasma.
29) Trained nearly 200 graduate students in fusion science, engineering, and plasma physics.

ACKNOWLEDGEMENTS

This work has been supported by U.S. Department of Energy Agreements DE-FC02-99ER54512 and DE-SC0014264.

REFERENCES

[1.1] I. Hutchinson, et al., Phys. Plasma **1**(1994)1511.
[1.2] E. Marmar, et al., Fusion Sci. Technol. **51**(2007)261.
[1.3] M. Greenwald, et al., Physics of Plasmas **21**(2014)110501.
[2.1] P. Rodriguez-Fernandez, et al., this conference.
[2.2] G.M. Staebler, et al., Nucl. Fusion **57** (2017) 066046.
[3.1] J.W. Hughes, et al., Nucl. Fusion **58**(2018) 112003.
[3.2] P.B. Snyder, et al., Nucl. Fusion **55** (2015) 083026.
[3.3] A. Hubbard, et al., Nucl. Fusion **57**(2017)126039.
[3.4] https://www.psfc.mit.edu/research/topics/sparc
[3.5] B.N. Sorbom, et al., Fusion Eng. and Design **100**(2015)378.
[3.6] Y. Ma,et al., Nucl. Fusion **52** (2012) 023010.
[3.7] E. Tolman, et al., Nucl. Fusion **58** (2018) 046004.
[3.8] M. Schmidtmayr, et al., Nucl. Fusion **58** (2018) 056003.
[3.9] F. Ryter, et al., Nucl. Fusion **54** (2014) 083003.
[3.10] Y. Martin, et al., J. Phys Conf. Series **123** (2008) 012033.
[4.1] S. G. Baek et al., Physical Review Letters 121, (2018) 055001.
[4.2] P.T. Bonoli et al., High Field Side Lower Hybrid Wave Launch for Steady State Plasma Sustainment, Nuclear Fusion (in press, 2018).
[4.3] Y. Takase et al., Phys. Fluids 28 (1985) 983.
[4.4] G.M. Wallace et al., Physics of Plasmas 17 (2010) 082508.
[4.5] R. Cesario et al., Nature Communications 1 (2010) 1.
[4.6] Gregory M. Wallace, MIT PhD thesis, 2009, http://hdl.handle.net/1721.1/57694
[4.7] S. G. Baek et al., Plasma Phys. Control. Fusion, **55**(2013) 052001.
[4.8] I. C. Faust et al., Phys. Plasmas, **23**(2016 056115.
[5.1] D. Brunner, B. LaBombard, A.Q. Kuang and J.L. Terry, Nucl. Fusion **58**(2018)094002.
[5.2] B. LaBombard, et al., Nucl. Fusion **55** (2015) 053020.
[5.3] M.V. Umansky et al., Phys. Plasmas **24** (2017) 056112
[5.4] M.V. Umansky et al., this conference.
[5.5] E.A. Tolman et al., this conference.
[5.6] M. Wigram et al., this conference.
[5.7] G.M. Wallace, et al., this conference.
[5.8] T. Eich, et al., Nucl. Fusion **53** (2013) 093031.
[5.9] T. Golfinopoulos, et al., Nucl. Fusion **58**(2018)056018.

[6.1] M. Hoppe, O. Embreus, R.A. Tinguely, R.S. Granetz, A. Stahl and T. Fulop, Nucl. Fusion **58**(2018) 026032.
[6.2] R.A. Tinguely, R.S. Granetz, M. Hoppe and O. Embreus, Nucl.Fusion **58**(2018)076019.
[6.3] R.A. Tinguely, R.S. Granetz, A. Berg, A.Q. Kuang, D. Brunner, and B. LaBombard, Nucl. Fusion **58**(2018)016005.
[6.4] R.S. Granetz, et al., this conference.
[7.1] J. Irby, D. Gwinn, W. Beck, B. LaBombard, R. Granetz, and R.Vieira, FusionSci.Technol.**51**(2007)460.
[7.2] I.H.Hutchinson, et al.,Phys.Plasmas **1**(1994)1511.
[7.3] J.L. Terry, B. LaBombard, B. Lipschultz, M.J. Greenwald, J.E. Rice, and S.J. Zweben, Fusion Sci. Technol. **51**(2007)342.
[7.4] B. Lipschultz, B.LaBombard,J.L. Terry,C. Boswell,and I.H. Hutchinson, FusionSci.Technol. **51**(2007)369.
[7.5]W.R.Wampler,et al., Proceedings of 18th IEEE Symposium on Fusion Engineering **1**(1999)267.
[7.6] H.S.Barnard,B.Lipschultz,andD.G.Whyte,J.Nucl.Mater. **415**(2011)S301.
[7.7] B. Lipschultz, D.G. Whyte, J. Irby, B. LaBombard, and G.M. Wright, Nucl. Fusion **49**(2009)045009.
[7.8] B. Lipschultz, D.B. Montgomery, P.A. Politzer and S.M. Wolfe, J.Nucl.Mater. **121**(1984)441.
[7.9] B. Lipschultz, B. LaBombard, J.L. Terry, C. Boswell,and I.H. Hutchinson, Fusion Sci. Technol. **51**(2007)369.
[7.10] J.L.Terry, et al., At. Processes Plasmas **443**(1998)43.
[7.11] B. LaBombard, et al., Nucl.Fusion **40**(2000)2041.
[7.12] J.A. Goetz, et al., Phys. Plasmas **6**(1999)1899.
[7.13] J.W. Hughes, et al., Nucl. Fusion **51**(2011)083007.
[7.13] A. Loarte, et al., Phys.Plasmas **18**(2011)056105.
[7.15] B. LaBombard, et al., Phys. Plasmas **8**(2001)2107.
[7.16] B. LaBombard, et al., Nucl. Fusion **45**(2005)1658.
[7.17] B. LaBombard, et al., Phys. Plasmas **8**(2001)2107.
[7.18] M. Greenwald, Plasma Phys. Controlled Fusion **44**(2002)R27.
[7.19] B. LaBombard, et al., Phys. Plasmas **12**(2005)056111.
[7.20] J.E. Rice, et al., Nucl. Fusion **45**(2005)251.
[7.21] A.E. Hubbard, et al., Proc. 16th IAEA Conf. on Fusion Energy, Montreal **1**(1996)875.
[7.22] A.E. Hubbard, et al., Plasma Phys. Controlled Fusion **40**(1998)689.
[7.23] D.G. Whyte, et al., Nucl. Fusion **50**(2010)105005..
[7.24] A.E. Hubbard, et al., Phys. Plasmas **18**(2011)056115.
[7.25] M. Greenwald, et al., Plasma Phys. Controlled Fusion **42**(2000)A263.
[7.26] M. Greenwald, etal., Nucl.Fusion **37**(1997)793.
[7.27] D. Mikkelsen, et al., Proc. 19th IAEAFusionEnergyConference(2002), http://www-pub.iaea.org/MTCD/publications/PDF/csp_019c/pdf/exp5_03.pdf
[7.28] J.E.Rice, et al., Nucl. Fusion **38**(1998)75.
[7.29] J.E. Rice, et al., Phys. Rev. Lett. **106**(2011)215001.
[7.30] S.J. Wukitch, et al., Phys. Plasmas **9**(2002)2149.
[7.31] C.L. Fiore, et al., Phys. Plasmas **19**(2012)056113.
[7.32] J.E. Rice, et al., Nucl. Fusion **42**(2002)510.
[7.33] C.L. Fiore, et al., Plasma Phys. Controlled Fusion **46**(2004)B281.
[7.34] D.R. Ernst, et al., Phys. Plasmas **11**(2004)2637.
[7.35] N.T. Howard, et al., Phys. Plasmas **19**(2012)056110.
[7.36] N.T. Howard, A.E. White, M. Greenwald, C. Holland, and J.Candy, Phys. Plasmas **21**(2014)032308.
[7.37] J.E. Rice, et al.,Nucl. Fusion **37**(1997)241.
[7.38] M.L. Reinke, et al., ,Nucl. Fusion **53**(2013)043006.
[7.39] J.E. Rice, et al., J. Phys. B: At., Mol. Opt. Phys. **47**(2014)075701.
[7.40] S.J. Wukitch, et al., Phys. Plasmas **20**(2013)056117.
[7.41] P.T. Bonoli, et al., Fusion Sci. Technol. **51**(2007)401.
[7.42] V. Tang, et al., Plasma Phys. Controlled Fusion **49**(2007)873.
[7.43] A. Bader, et al., Nucl. Fusion **52**(2012)094019.
[7.44] P.J. O'Shea, et al., Proc. 11th Conf. on Radio Frequency Power in Plasmas (AIP,1997),Vol.**403**,p.89.
[7.45] N. Tsujii, et al., Phys. Plasmas **19**(2012)082508.
[7.46] Y. Lin, et al., Phys. Rev. Lett. **101**(2008)235002.
[7.47] S.J. Wukitch, et al., Phys. Plasmas **20**(2013)056117.
[7.48] S.Shiraiwa, et al., Nucl. Fusion **51**(2011)103024.
[7.49] J.R.Wilson, et al., Nucl. Fusion **49**(2009)115015.
[7.50] J.C.Wright, et al., Phys. Plasmas **11**(2004)2473.
[7.51] G.M.Wallace et al., Phys. Plasmas **17**(2010)082508.
[7.52] O.Meneghini, S. Shiraiwa, and R. Parker, Phys. Plasmas **16**(2009)090701.
[7.53] S.G.Baek et al., Phys. Plasmas **21**(2014)012506.
[7.54] S.Shiraiwa, et al., Phys. Plasmas **18**(2011)080705.
[7.55] R.S. Granetz,et al., Nucl. Fusion **36**(1996)545.
[7.56] G.M. Olynyk,et al., Nucl. Fusion **53**(2013)092001.